



# Photoelectrochemical cathodic protection of amorphous zinc oxide coating on hot rolled steel SS400 in a 3 wt% NaCl solution and a Na<sub>2</sub>S-NaOH solution

Phatchara WIPATAPHAN<sup>1</sup>, Worapot SRIPIANEM<sup>1</sup>, Naw BLESSING OO<sup>1,2</sup>, Thanate NA WICHEAN<sup>1,3</sup>, Boossayamas DACHBUMROONG<sup>1,3</sup>, Oratai JONGPRATEEP<sup>1,2</sup>, Gasidit PANOMSUWAN<sup>1,2</sup>, Naray PEWNIM<sup>1,2</sup>, Ratchatee TECHAPIESANCHAROENKIJ<sup>1,2,3,\*</sup>

<sup>1</sup>Department of Materials Engineering, Faculty of Engineering, Kasetsart University, 50 Ngamwongwan Rd, Chatuchak, 10900, Bangkok, Thailand.

<sup>2</sup>International Collaborative Education Program for Materials Technology, Education, and Research (ICE-Matter), ASEAN University Network/Southeast Asia Engineering Education Development Network (AUN/SEED-Net), Faculty of Engineering, Kasetsart University, 50 Ngamwongwan Rd, Chatuchak, 10900, Bangkok, Thailand.

<sup>3</sup>Materials Innovation Center, Faculty of Engineering, Kasetsart University, Bangkok 10900, Thailand

\*Corresponding author e-mail: fengrct@ku.ac.th

## Received date:

10 August 2021

## Revised date:

21 October 2021

## Accepted date:

28 October 2021

## Keywords:

Photocathodic protection;  
Corrosion;  
Hole scavenger;  
Thin film;  
Zinc oxide

## Abstract

The photoelectrochemical cathodic protection of amorphous ZnO thin-film coating on hot rolled steel SS400, in the 3 wt% NaCl environment, was investigated. The ZnO thin film was coated on a SS400 substrate at 200°C using the spray pyrolysis technique. The x-ray diffractometry analysis confirmed the amorphous ZnO coatings. Two different types of the electrochemical cells were used: a single-cell and a double-cell system. Two different types of the photoelectrolytic solutions were compared: (i) 0.1 M Na<sub>2</sub>S + 0.2 M NaOH and (ii) 3 wt% NaCl solution. The ZnO-coated SS400 samples were subjected to potentiostatic polarization testing under dark and UV conditions, with the immersion of either Na<sub>2</sub>S-NaOH or NaCl solution. The photoelectrochemical analysis showed that the photocathodic protection on SS400 by the ZnO coating could be demonstrated with the photoelectrolytic solution of Na<sub>2</sub>S-NaOH. The voltage was negatively shifted and the current density was increased with the UV irradiation on the ZnO coating, immersing in the Na<sub>2</sub>S-present solution. The ZnO coating was also stable in the Na<sub>2</sub>S-NaOH solution. The microstructural analyses with Optical Microscope and Scanning Electron Microscope were conducted to support the photoelectrochemical analyses.

## 1. Introduction

Steels are one of the most widely used metals in industrial and engineering structures due to their availability, excellent mechanical properties and machinability. However, steels exhibit poor corrosion resistance due to their electrochemical activity in aqueous environments [1-7]. Cathodic protection and coatings are the two most widely applied technologies for preventing corrosion on a steel [8]. Cathodic protection is a technique that supplies electrons to a steel for corrosion protection from an external source, so the protected steel becomes more cathodic and higher corrosion-resistant. It can be distinguished into 2 types: impressed current cathodic protection and sacrificial anode. The impressed current CP is a technique that uses an ohmic connection from an external power supply to supply electrons and polarize a protected steel to the corrosion stable region. The sacrificial anode CP is a technique that connects active metals (more anodic) such as zinc and aluminum with the protected steel. Then, the coupled active metals act as anodes supplying electrons to the protected steel to prevent corrosion. However, there are some limitations for CP techniques, such as an unavailability of power supplies in remote areas for the

impressed current CP, or a limited-service lifetime for the sacrificial anode CP [2].

In recent years, the photocathodic protection system has attracted attention due to its exhibition of a cathodic protection for a metal under solar light illumination [9-12]. This system exhibited the protection without using either external electric power or a sacrificial anode material by applying an n-type semiconductor film to provide cathodic protection on a metal, using inexhaustible solar energy for electron generation [12,13-27]. During the photocathodic protection process, the n-type semiconductor acts as a non-sacrificed photoanode that provides photo-generated electrons to a protected metal. Photocathodic protection is environmentally-friendly and can be applied either by a direct coating [14-16,28,29] or as a coupling cell [18,30-32].

The photocathodic protection was early reported by Imokawa, *et al.* [33] with the photocathodic protection effect of TiO<sub>2</sub> films. The results demonstrated that during the irradiation with ultraviolet (UV) light, the presence of electron-hole pairs (EHPs) in titanium dioxide (TiO<sub>2</sub>) film (band gap energy of 3.2 eV) occurred and the OCP of the coupled metal shifted to the negative potential, which lowered and even prevented the corrosion of the coupled metal. Another important early report,

from Yuan and Tsujikawa [25], is the photocathodic protection of Cu by coating TiO<sub>2</sub> to prevent corrosion under UV illumination. It demonstrated that, under UV on, electron-hole pairs occurred in the TiO<sub>2</sub> coating and subsequently were transferred into the Cu substrate for a cathodic reaction and preventing an oxidation of Cu to Cu ions. As a result, the TiO<sub>2</sub> coating acts as a non-sacrificial anode and Cu acts as a cathode. For both reports, it demonstrated that the photocathodic protection, without the dissolution of either the n-type semiconductor coating or a metal, was feasible and effective for copper [34], stainless steel [10,12,19,22,33,35-37] and carbon steel [38,39].

The photocathodic protection may be explained by the photoelectrochemical mechanism of a semiconductor film and a metal in an electrolytic system. The electrons from valence band (VB) of an n-type semiconductor are excited into the conduction band (CB) by the absorption of photons, resulting in holes in the VB of the semiconductor. The photo-generated electrons can migrate to the metal, when the CB level of the n-type semiconductor is higher than the Fermi energy (FE) level of the metal. The transferred electrons then enable a cathodic reaction on the metal surface to suppress or prevent the corrosion, while the remaining holes play a part in an anodic reaction on the n-type semiconductor coating with an environmental solution. As a result, if the electron-generating and electrons-transfer rates are higher than the electron-consuming rate by oxidizing species, then the metal becomes stable and more cathodic. The transferred electrons are enriched in the metal, then compensate for the corrosion current and polarize the potential of metal to a more negative and stable region [2,38]. Accordingly, an n-type oxide semiconductor which can absorb UV and visible lights and have a higher FE level than that of a metal can provide the photoelectrochemical cathodic protection to the metal [40,41]. So far, different n-type semiconductor oxides with wide band gap have been reported to be good candidates as a photosensitive material for photocathodic protection, such as TiO<sub>2</sub> [42-46], SnO<sub>2</sub> [47], ZnO [48], WO<sub>3</sub> [49] and SrTiO<sub>3</sub> [24,50].

ZnO is one of the ideal n-type semiconductor materials for the photocathodic protection, with high photocatalytic activity, abundance with simple synthesis, low toxicity, and low cost. ZnO has a proper band gap energy of 3.37 eV that can absorb UV and visible lights and 375 nm absorption wavelengths that contribute to transparency of ZnO [51,52]. Techapiesanchaorenkij *et al.* [48] reported that the photocathodic characteristics of the amorphous and crystalline ZnO thin films coated on SS304 in a 3 wt% NaCl solution under UV light illumination. The results showed that, under UV light on, the open circuit potential (OCP) of the amorphous ZnO-coated SS304 shifted toward more negative than that of the bare SS304, and the OCP returned to the same value after UV light off. The electrons could be generated in the ZnO coating under UV light on and migrated to SS304, providing a photocathodic protection to the SS304. The report has demonstrated the possibility of using an ZnO as a photocathodic protection coating.

However, one of the main issues of an n-type semiconductor, which can decrease the cathodic protection performance, is a recombination of electron-hole pairs (EHP's). If there is no hole trapping agent in the environment medium, the anode depolarization process will be inhibited, which will increase the difficulty of separation process of the photo-generated electron-hole pairs. To overcome this problem, one alternative strategy is using hole scavenger solutions such as

Na<sub>2</sub>S [37,41,50,53,54], which readily oxidize with holes at the interface of the semiconductor and the electrolyte.

Yang and Cheng [50] reported the effect of SrTiO<sub>3</sub> photoanode for photocathodic protection of stainless steel AISI 304 and X52 carbon steel immersed in two different hole scavengers that are 0.1 M Na<sub>2</sub>S + 0.2 M NaOH solution and a 3.5 wt% NaCl solution. In the Na<sub>2</sub>S-NaOH solution, NaOH act as the preventer for Na<sub>2</sub>S hydrolysis and Na<sub>2</sub>S acts as the hole scavenger, while, in the NaCl solution, NaCl act as supporting and H<sub>2</sub>O acts as the hole scavenger electrolyte. The results demonstrated that, under both UV and dark conditions, the current density of SrTiO<sub>3</sub> in Na<sub>2</sub>S-NaOH solution was higher than the current density of SrTiO<sub>3</sub> in the NaCl solution. Na<sub>2</sub>S helped prevent the recombination of EHP's [35,55,56] by reacting of produced holes with S<sup>2-</sup> and the excitation of produced electrons into the CB, resulting in a more photo current density [50].

Sun *et al.* [41] reported the effects of the coupling of ZnO thin film photoanode to Zn, Q235 carbon steel, and stainless steel AISI 304 photocathodic protection in 3.5 wt% NaCl solution under light illumination. In the presence of Na<sub>2</sub>S, the results show that the potential was shifted with higher negative potential, which occurred by the prevention of electron-hole pair recombination from S<sup>2-</sup> ion that can capture produced holes. For this case, the OCP of ZnO was more negative than OCP of zinc, Q235 carbon steel and stainless steel AISI 304. In the absence of Na<sub>2</sub>S, the results show that the potential was shifted with lower negative potential due to the high energy barrier of the anodic reaction, which occurred by the recombination of ZnO produced holes and electrons. The resultant OCP of ZnO is still more positive than those of zinc and Q235 carbon steel. As a result, without Na<sub>2</sub>S, the ZnO can provide the photocathodic protection for only stainless steel AISI 304. The report demonstrated that ZnO could provide photocathodic protection for the Q235 carbon steel with the assistance of Na<sub>2</sub>S [41].

To date, there is no report of the photocathodic characteristics of a ZnO coating on hot rolled steel substrate with two different solutions, NaCl-based and Na<sub>2</sub>S-NaOH-based solutions, on the opposing ZnO-coated and bare sides of the same sample, using direct coating techniques. In this work, the photocathodic characteristics of an amorphous ZnO coating on a hot rolled steel SS400 were investigated. The ZnO thin films were deposited on SS400 via the spray pyrolysis technique. The spray pyrolysis technique can fabricate ZnO thin film at a large scale with fast and effective cost [40,48,56-58]. A double-cell electrochemical setup was applied, so the ZnO-coated side of SS400 and the opposing bare SS400 side were immersed in different solutions: Na<sub>2</sub>S-NaOH and NaCl solutions. The potentiostatic polarization and open-circuit potential (OCP) tests under dark and UV conditions were investigated on the ZnO-coated SS400 for the photocathodic characteristics. The morphological and phase analyses were also investigated to support the photoelectrochemical cathodic study.

## 2. Materials and method

The amorphous ZnO thin films were produced by the pneumatic spray pyrolysis technique [59]. A 3 × 3 cm<sup>2</sup> hot rolled steel SS400 substrate was cleaned by using ultrasonic cleaner with deionized water (DI water), acetone and ethanol for 10 min each. For the precursor solution, 0.05 M zinc acetate dihydrate was dissolved in a methanol

solvent with magnetic stirring for 10 min. The precursor solution was fed into a syringe pump at 4 mL·min<sup>-1</sup> and mixed with a carrier gas at a spray nozzle to form micro-droplet sprays. This micro-droplet solution was sprayed on the cleaned substrate. The spraying time and substrate temperature were set at 10 min and 200°C, respectively.

The microstructures of the amorphous ZnO thin films were analyzed and confirmed by an Optical microscope (OM, DM2700M Lica) and a Scanning electron microscope (SEM, FEI Quanta 450). The elemental analyses were performed by an Energy dispersive x-ray spectroscopy (EDS). The crystalline structures of the ZnO thin films were analyzed and recorded by X-ray diffractometry (XRD, Phillips X'Pert) with Cu-K $\alpha$  radiation with the 2 $\theta$  angular range from 20° to 80°.

The photoelectrochemical characteristics of the ZnO-coated SS400 samples were investigated under two different conditions: (i) a single-cell condition (Figure 1) and (ii) a double-cell condition

(Figure 2). For the single-cell condition, shown in Figure 1, one side of the SS400 sample was immersed in an electrolytic cell along with a Pt-coated counter electrode and an Ag/AgCl reference electrode. The other side of the SS400 sample was sealed with Teflon tape. The electrochemical responses of two different samples, Bare SS400 and ZnO-coated SS400 samples, in two different electrolyte solutions (i) 3 wt% NaCl (NaCl solution) and (ii) 0.1 M Na<sub>2</sub>S + 0.2 M NaOH solutions (Na<sub>2</sub>S-NaOH solution), were measured. The photoelectrochemical responses were measured under dark and UV illumination. For the dark condition, the cell was under a closed chamber without any light. For the UV condition, the UV light was illuminated directly on the active surface in the electrolytic cell. The light UVA irradiation source was provided by OSRAM 300 W that has a wavelength of 315 nm to 380 nm. The electrolyte temperature was controlled at room temperature for all measurements.

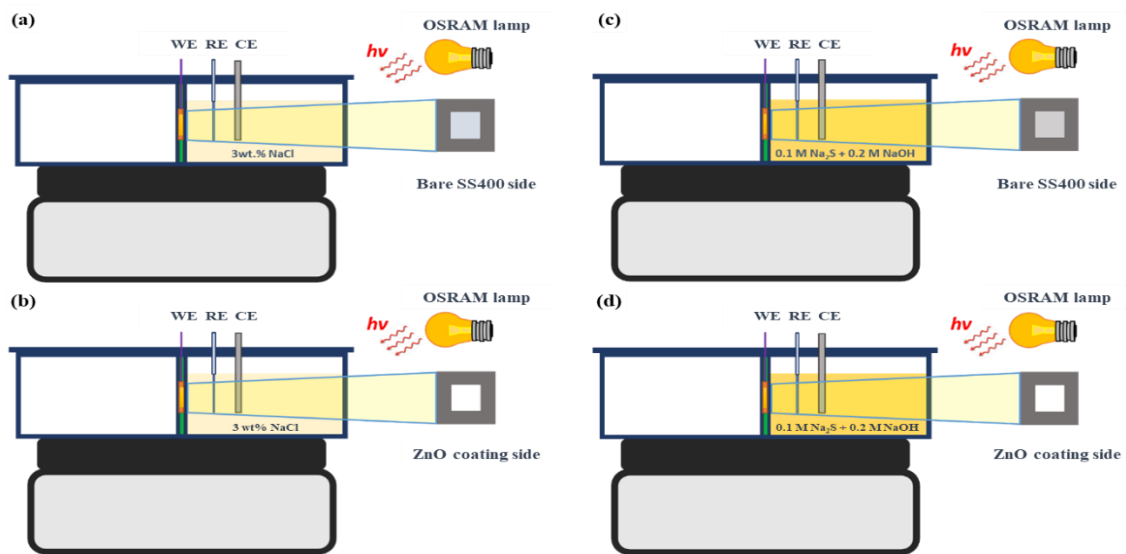


**Figure 1.** Single-cell setups for: (a) bare SS400 side in a NaCl solution, (b) ZnO-coated SS400 side in a NaCl solution, (c) bare SS400 side in a Na<sub>2</sub>S-NaOH solution, and (d) ZnO-coated SS400 side in a Na<sub>2</sub>S-NaOH solution.

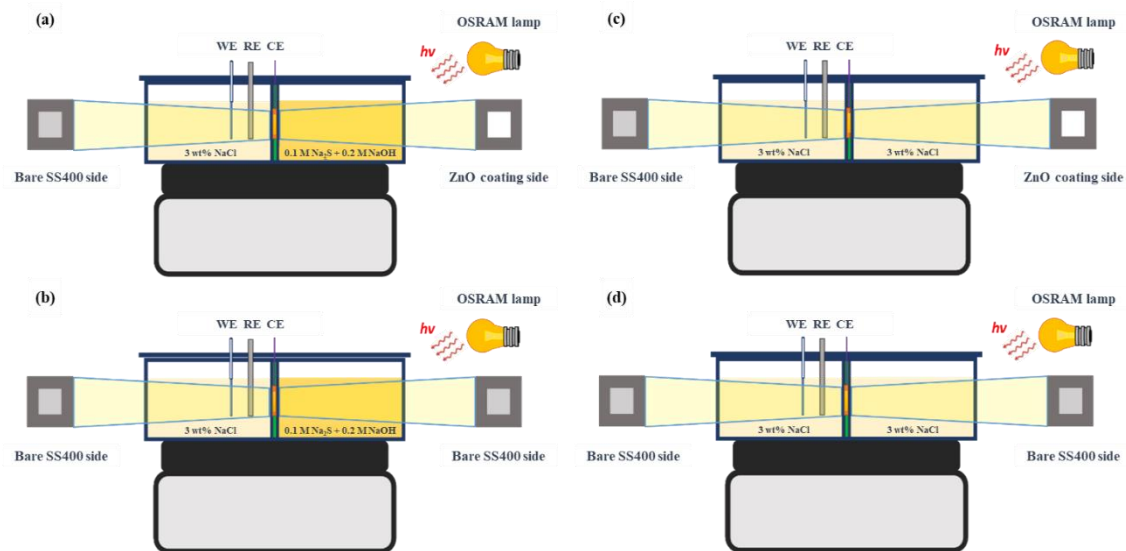


**Figure 2.** Double-cell setups for: (a) bare SS400 side in NaCl solution and its opposing ZnO-coated side in Na<sub>2</sub>S-NaOH solution, (b) two bare SS400 sides in NaCl and Na<sub>2</sub>S-NaOH solutions, (c) bare and ZnO-coated SS400 sides in NaCl solutions, and (d) two bare SS400 sides in NaCl solutions.

For the double-cell condition, as shown in Figure 2, two sides of the SS400 samples were exposed in two opposite electrolytic cells. The double-cell system was composed of a corrosion cell and a photoelectrolytic cell. For the corrosion cell, the electrolyte was a NaCl solution. The uncoated SS304 side was a working electrode, exposed in the corrosion cell, along with the Pt-coated counter electrode and Ag/AgCl reference electrode. The NaCl solution acted as a Cl<sup>-</sup>-environment corrosive solution to the bare SS400 side. For the photoelectrolytic cell, the main electrolyte in the photoelectrolytic cell is a 3 wt% NaCl solution (NaCl) or a 0.1 M Na<sub>2</sub>S + 0.2 M NaOH solution (Na<sub>2</sub>S-NaOH). The ZnO-coated side was exposed in the photoelectrolytic cell. And, for UV condition, the UV light was illuminated on the ZnO-coated side in this cell (as illustrated in Figure 2). The photoelectrolytic cell was designed for the photocatalytic activity, in which the Na<sub>2</sub>S-NaOH solution provided hole-scavenging species to the ZnO coated side and the photo-generated electron-hole pairs (EHPs) would provide photocathodic protection to the opposite uncoated SS400 side, exposed in the corrosion cell. The photoelectrochemical study was conducted under dark and UV conditions. The light UVA irradiation source was provided by OSRAM 300 W that has a wavelength 315 nm to 380 nm. The effective photon wavelength for the ZnO bandgap of 3.37 eV is 336 nm that is suitable for UVA because UVA can irradiate through the atmosphere to earth by sunlight irradiation. For controlled conditions, an uncoated SS400 sample and a NaCl solution were used in the photoelectrolytic cell in place of ZnO-coated sample and a Na<sub>2</sub>S-NaOH solution, respectively.

The photoelectrochemical measurements were performed by using Metrohm Autolab Potentiostatic / Galvanostatic with NOVA interface software. The effective area of the sample was 1 × 1 cm<sup>2</sup> that was used as a working electrode while the counter and reference electrodes were a Pt-coated steel mesh and Ag/AgCl, respectively. For the double-cell condition, all three electrodes were immersed in the corrosion cell of a 3 wt% NaCl solution. Two photoelectrochemical analyses were measured: (i) the potentiodynamic polarization analysis and (ii) the UV effect on the open circuit potential (OCP). The potentiodynamic polarization curves were recorded in the range of -0.5 V and 0.5 V vs. OCP at a potential scan rate of 0.001 V·s<sup>-1</sup>, under dark and UV conditions. Tafel extrapolation was evaluated on the polarization curves to estimate the corrosion potential ( $V_{\text{corr}}$ ) and current density ( $i_{\text{corr}}$ ). For the UV effect on OCP, the OCP of the samples in a NaCl solution and Na<sub>2</sub>S-NaOH solution were performed to observe the change of OCP value as the UV lights were switching on and off in different solutions.

For the photoelectrochemical characterization, two types of the samples (bare SS400 and ZnO-coated SS400) with two different systems (single-cell and double-cell systems) were investigated, as illustrated in Figure 1 and Figure 2. For systematic comparison, these conditions are labeled as followings: (i) SS400 sample with no coating in the single-cell system, labeled as 1SS400, (ii) SS400 sample with no coating in the double-cell system, labeled as 2SS400, (iii) SS400 with amorphous ZnO coating on one side in the single-cell system, labeled as 1SS400 Amorphous and (iv) SS400 with amorphous ZnO coating on one side in the double-cell system, labeled as 2SS400 Amorphous.

### 3. Results and discussion

#### 3.1 Morphological, compositional and structural characterizations of the ZnO coatings

The ZnO thin films, coated on a SS400 sample by spray pyrolysis at 200°C for 10 min, exhibited a white tint transparent film with a similar color to the bare SS400, as compared in Figure 3(a) and (b). The OM microstructures of the ZnO coatings on SS400 and the bare SS400 are shown in Figure 4. The ZnO coating film is thin and transparent so that the optical microstructures appear similar to the bare SS400 surface.

The SEM microstructures of the ZnO coatings on SS400 are shown in Figure 5. The ZnO thin film exhibited a smooth uniform coating on the SS400 substrate. The microstructure of the ZnO thin films exhibited amorphous-like, nano-powdery and non-crystalline structure with average particle size of 16 nm.

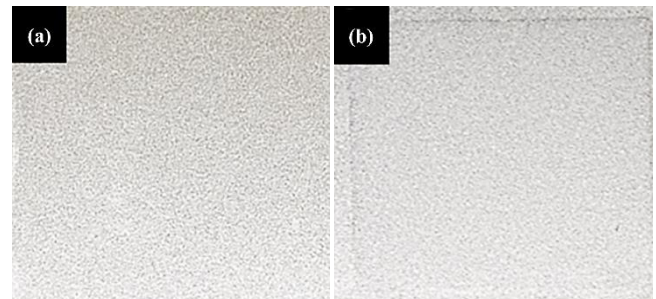


Figure 3. Pictures of (a) the bare SS400, and (b) the ZnO-coated SS400.

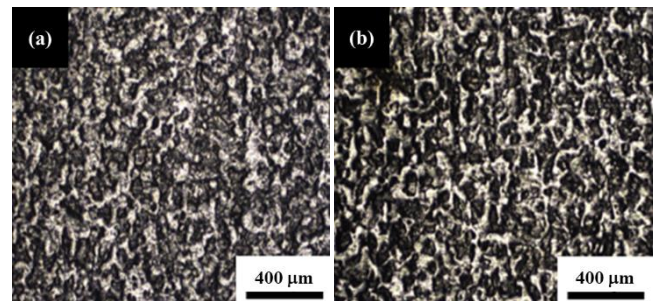


Figure 4. OM microstructures of: (a) bare SS400 magnification 50x, and (b) amorphous ZnO thin film coated on SS400 magnification 50x.

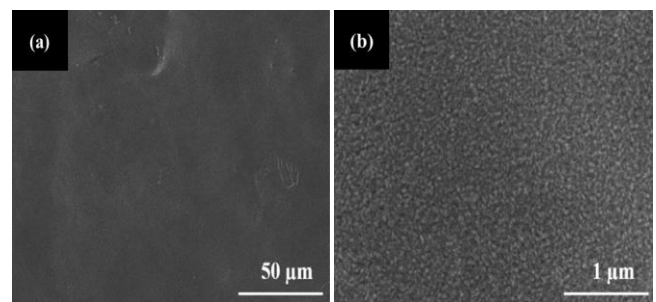


Figure 5. SEM microstructures of the ZnO thin film coated on SS400: (a) magnification 1,000x (b) magnification 40,000x.

The representative XRD patterns of the amorphous ZnO coatings on SS400 are shown in Figure 6. For the amorphous ZnO thin films, the respective diffraction peaks with preferential planes match with the standard JCPDS ZnO peaks. It shows broad diffraction peaks of ZnO at (002), (101), and (110) with 31°, 34° and 36° 2θ peaks, respectively. The preferential peaks are broad, indicating the disordered and non-crystalline ZnO structures. It is due to the fact that, during fabrication, the ZnO coating was sprayed at 200°C without subsequent annealing, contributing to the disordered and non-crystalline ZnO thin film on the SS400 substrate. The amorphous-like broad ZnO peaks correspond with the SEM microstructures of nano-powdery non-crystalline structures shown in Figure 5 above. The 2θ peaks of Fe are also present for both ZnO-coated and bare SS400 at 44° and 65°, which match with the respective diffraction peaks with preferential planes of (110) and (200) of the standard JCPDS Fe peaks.

### 3.2 Photoelectrochemical characteristics of the amorphous ZnO coatings on SS400 and the bare SS400 in the single-cell system

To study the photocathodic characteristic of Amorphous ZnO coating film, the corrosion potential ( $V_{\text{corr}}$ ) current density ( $i_{\text{corr}}$ ) and open circuit potential (OCP) of the ZnO-coated and bare SS400 are measured under dark and UV-illumination conditions. Two different electrolyte solutions were used, including a NaCl solution and a Na<sub>2</sub>S-NaOH solution. For the NaCl solution, NaCl acts as supporting electrolyte with Cl<sup>-</sup> ions as corrosive agents, while for the Na<sub>2</sub>S-NaOH solution, Na<sub>2</sub>S acts as the hole scavenger and NaOH is used to prevent Na<sub>2</sub>S hydrolysis.

The linear polarization curves of the ZnO-coated SS400 samples in the single-cell system (ISS400 Amorphous), under dark and UV conditions, are shown in Figure 7. The corrosion potential ( $V_{\text{corr}}$ ), current density ( $i_{\text{corr}}$ ) and open circuit potential (OCP) are summarized in Table 1. In the NaCl solution, the amorphous ZnO-coated SS400 showed the  $V_{\text{corr}}$  of -0.342 V (vs. Ag/AgCl) and  $i_{\text{corr}}$  of  $1.98 \times 10^{-5}$  A·cm<sup>-2</sup>, under dark conditions. With the UV on, the  $V_{\text{corr}}$  and  $i_{\text{corr}}$  of the amorphous ZnO coating were -0.348 V (vs. Ag/AgCl) and  $1.25 \times 10^{-5}$  A·cm<sup>-2</sup>, which are similar to those under the dark condition. In the Na<sub>2</sub>S-NaOH solution, under dark conditions, the cathodic and anodic polarizations were observed with  $V_{\text{corr}}$  of -0.454 V (vs. Ag/AgCl) and  $i_{\text{corr}}$  of  $9.89 \times 10^{-6}$  A·cm<sup>-2</sup>. With the UV on, the  $V_{\text{corr}}$  of amorphous ZnO thin film were shifted cathodically to -0.687 V (vs. Ag/AgCl), along with an increase in  $i_{\text{corr}}$  by 10 times as much as that of the dark condition. The potential became more cathodic and the current density was increased by UV illumination due to the fact that the UV absorption of the amorphous ZnO thin film produced EHP's, culminating in extra photocurrent [41,50].

**Table 1.** The corrosion potential ( $V_{\text{corr}}$ ), current density ( $i_{\text{corr}}$ ) and open circuit potential (OCP) of the ZnO-coated SS400 Amorphous in the single-cell system with either a NaCl solution or in a Na<sub>2</sub>S-NaOH solution.

Sample	Condition	$V_{\text{corr}}$ (V)	$i_{\text{corr}}$ (A·cm <sup>-2</sup> )	OCP (V)
ISS400 Amorphous in NaCl	UV	-0.348	1.25E-05	-0.302
	Dark	-0.342	1.98E-05	-0.386
ISS400 Amorphous in Na <sub>2</sub> S	UV	-0.687	8.57E-05	-0.638
	Dark	-0.454	9.89E-06	-0.426

For the bare SS400 samples in the single-cell system, the linear polarization curves under dark and UV conditions are shown in Figure 8. The corrosion potential ( $V_{\text{corr}}$ ) current density ( $i_{\text{corr}}$ ) and open circuit potential (OCP) are summarized in Table 2. In the NaCl solution, the cathodic and anodic polarizations were observed with  $V_{\text{corr}}$  of -0.364 V (vs. Ag/AgCl) under dark conditions. With the UV illumination, the  $V_{\text{corr}}$  of the bare SS400 sample was shifted negatively to -0.452 V (vs. Ag/AgCl), with a higher current density as compared with that of the dark condition. In the Na<sub>2</sub>S-NaOH solution, the  $V_{\text{corr}}$  of -0.644 V (vs. Ag/AgCl) was measured under dark conditions. With UV on, the  $V_{\text{corr}}$  of the bare SS400 sample was shifted negatively to -0.786 V (vs. Ag/AgCl), with a similar current density as compared with that of the dark condition.

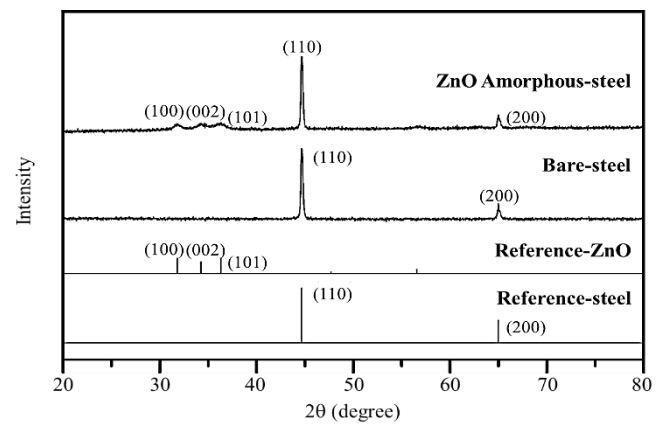


**Figure 6.** Representative XRD patterns of the amorphous ZnO thin films, Bare SS400, the standard reference of Zn and SS400 peaks are shown for analysis.

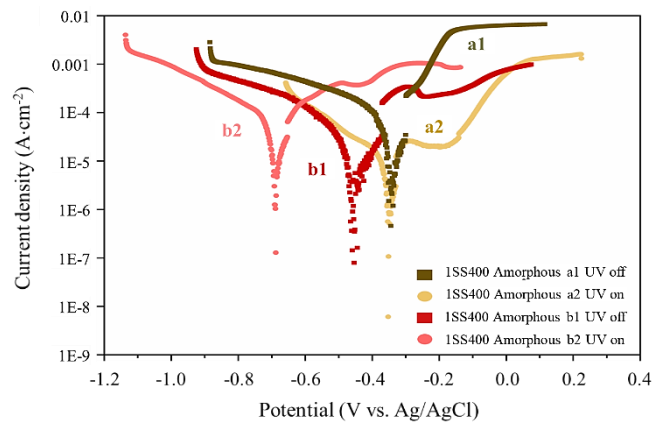


**Figure 7.** Linear polarization curves of the ZnO-coated SS400 samples in the single-cell system: SS400 Amorphous in a NaCl solution under dark (a1) and UV (a2) conditions, SS400 Amorphous in Na<sub>2</sub>S-NaOH solution under dark (b1) and UV (b2) conditions.

**Table 2.** The corrosion potential ( $V_{\text{corr}}$ ), current density ( $i_{\text{corr}}$ ) and open circuit potential (OCP) of the bare SS400 in the single-cell system with either a NaCl solution or a  $\text{Na}_2\text{S}$ -NaOH solution.

Sample	Condition	$V_{\text{corr}}$ (V)	$i_{\text{corr}}$ ( $\text{A}\cdot\text{cm}^{-2}$ )	OCP (V)
Bare SS400 in NaCl	UV	-0.452	2.17E-05	-0.486
	Dark	-0.364	8.95E-06	-0.428
Bare SS400 in $\text{Na}_2\text{S}$	UV	-0.786	5.68E-05	-0.642
	Dark	-0.644	1.85E-05	-0.604

The results were confirmed by the microstructure and surface investigation of the bare SS400 samples after the linear polarization measurement in the single-cell system, as evident in Figure 9(a-d), and Figure 10(a-d). In the NaCl solution, under either dark (Figure 9(a) and Figure 10(a)) or UV (Figure 9(b) and Figure 10(b)), the bare SS400 was corroded with pitting and uniform corrosion. On the other hand, in the  $\text{Na}_2\text{S}$ -NaOH solution, for either dark (Figure 9(c) and Figure 10(c)) or UV (Figure 9(d) and Figure 10(d)), the bare SS400 was stable without any visible sign of corrosion.

The results were confirmed by the microstructure and surface investigation of the amorphous ZnO-coated SS400 samples' exposed surfaces after the linear polarization measurement in the single-cell system, as evident in Figure 9(e-h) and Figure 10(e-h). In the 3 wt% NaCl solution, under either dark (Figure 9(e) and Figure 10(e)) or UV (Figure 9(f) and Figure 10(f)), the amorphous ZnO-coated SS400 samples were corroded with pitting and uniform corrosion. On the other hand, in the  $\text{Na}_2\text{S}$ -NaOH solution, either under dark (Figure 9(g) and Figure 10(g)) or UV (Figure 9(h) and Figure 10(h)), the amorphous ZnO-coated SS400 samples were stable without any visible corrosion. These results may be explained with the concept of photocathodic protection mechanism. In the  $\text{Na}_2\text{S}$ -NaOH solution, the band alignment of bare SS400 and ZnO thin film occurs to form Schottky contact effect. Under UV illumination, the photogenerated electrons from the amorphous ZnO coating were reacted with  $\text{H}^+$  and  $\text{O}_2$  in electron-transfer reactions resulting in higher current density, while the photogenerated holes were reacted with  $\text{S}^{2-}$  ion in  $\text{Na}_2\text{S}$ -NaOH solution.

With the elimination of holes with the hole-scavenger  $\text{S}^{2-}$ , the EHP's recombination could be reduced, resulting in more electrons for the redox reactions and higher current density [41,50]. For the dark condition, the ZnO coating was stable without any redox reaction in the  $\text{Na}_2\text{S}$ -NaOH solution, resulting in lower current density than the UV-condition counterpart. In the NaCl solution, the corrosion occurred, because the ZnO coating was unstable in an alkali solution and lost electron to NaCl in electron-transfer reactions, resulting in higher current density for both UV and dark condition [48].

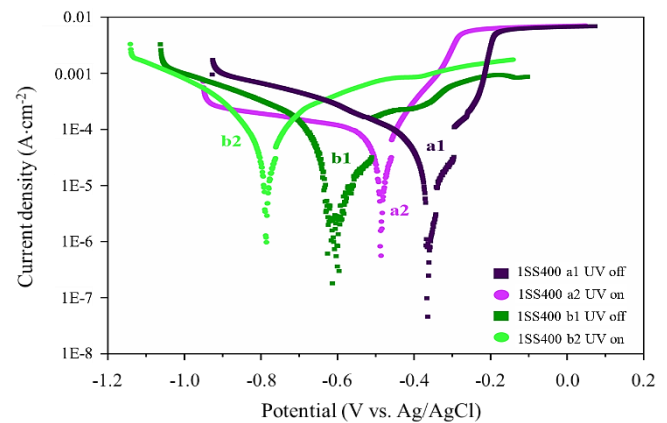


**Figure 8.** Linear polarization curves of the bare SS400 samples in the single-cell system. The bare SS400 in a NaCl solution under dark (a1) and UV (a2) conditions. The bare SS400 in a  $\text{Na}_2\text{S}$ -NaOH solution under dark (b1) and UV (b2) conditions.

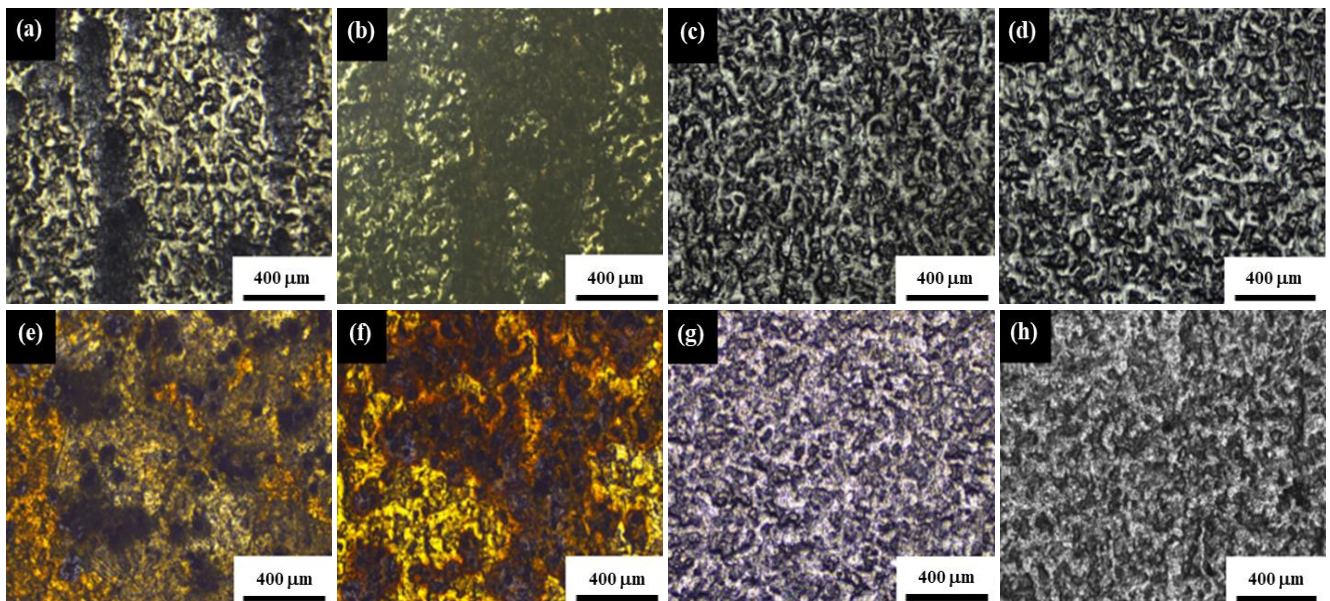


**Figure 9.** OM microstructures of the exposed surfaces after the linear polarization measurement in the single-cell system. Bare SS400 sample: (a) – (b) in NaCl and (c) – (d) in  $\text{Na}_2\text{S}$ -NaOH. ZnO-coated SS400 Amorphous: (e) – (f) in NaCl and (g) – (h) in  $\text{Na}_2\text{S}$ -NaOH.

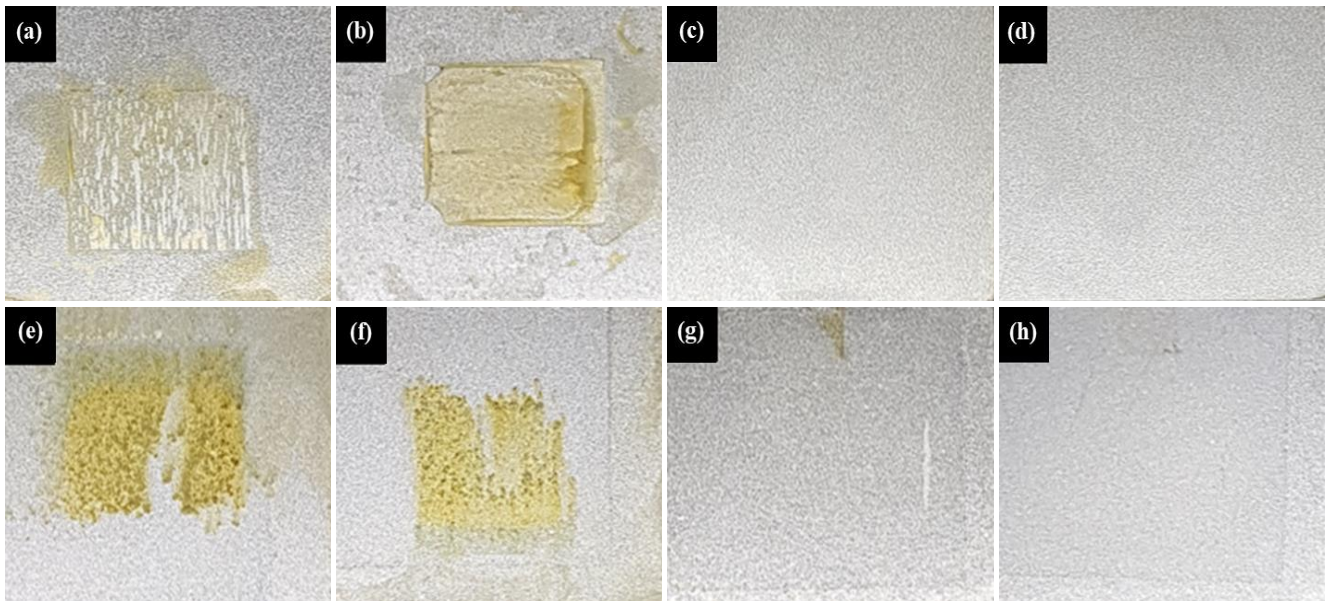


**Figure 10.** Digital pictures of the exposed surfaces after the linear polarization measurement in the single-cell system. Bare SS400 sample: (a) – (b) in NaCl and (c) – (d) in Na<sub>2</sub>S-NaOH. ZnO-coated SS400 Amorphous: (e) – (f) in NaCl and (g) – (h) in Na<sub>2</sub>S-NaOH.

### 3.3 Photoelectrochemical characteristics of the amorphous ZnO coatings on SS400 and the bare SS400 in the double-cell system

The linear polarization curves of the amorphous ZnO-coated SS400 samples, under either dark or UV conditions in the double-cell systems, are shown in Figure 11. The corrosion potential ( $V_{\text{corr}}$ ), current density ( $i_{\text{corr}}$ ) and open circuit potential (OCP) of SS400 Amorphous in NaCl, with the bare SS400 side in the NaCl corrosion cell and the ZnO-coated side in the NaCl photoelectrolytic cell, are shown in Table 3 (ii). And,  $V_{\text{corr}}$ ,  $i_{\text{corr}}$ , and OCP of SS400 Amorphous in NaCl and Na<sub>2</sub>S-NaOH double cell, with the bare SS400 side in the NaCl corrosion cell and the ZnO-coated side in the Na<sub>2</sub>S-NaOH photoelectrolytic cell, are shown in Table 3 (iii). From Figure 11 (Curve a1 and a2), with the NaCl solution in both corrosion and photoelectrolytic cells, the cathodic and anodic polarizations were observed with  $V_{\text{corr}}$  of -0.487 V (vs. Ag/AgCl) under dark conditions (Curve a1). With UV illumination (Curve a2), the  $V_{\text{corr}}$  is slightly shifted to -0.473 V (vs. Ag/AgCl), with similar current density compared to that of the dark condition. From Figure 11 (Curve b1 and b2), with the NaCl solution in the corrosion cell and the Na<sub>2</sub>S-NaOH solution in the photoelectrolytic cell, the cathodic and anodic polarizations were observed with  $V_{\text{corr}}$  of -0.561 V (vs. Ag/AgCl) under dark conditions (Curve b1). With the UV illumination (Curve b2), the  $V_{\text{corr}}$  is shifted

negatively to -0.595 V (vs. Ag/AgCl), with similar current density compared to that of the dark condition.

The UV illumination on the electrolytic-cell sides seemed to exhibit a small effect on the voltage and current density of the corrosion-cell sides. On the other hand, the solution type in the photoelectrolytic cell exhibited a significant effect on the voltage and current density.

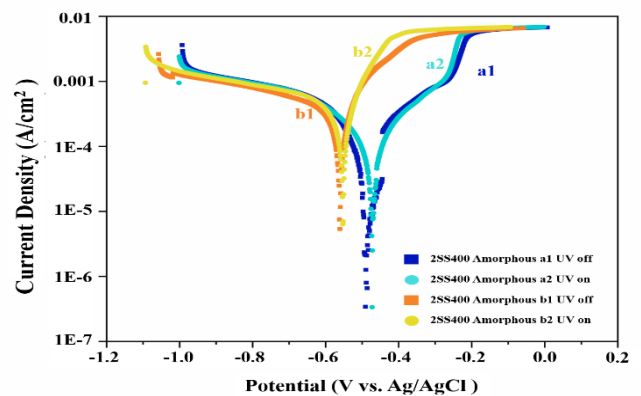


**Figure 11.** Linear polarization curves of the samples in the double-cell system. The SS400 Amorphous in NaCl double cells under dark (a1) and UV (a2). The SS400 Amorphous in NaCl and Na<sub>2</sub>S-NaOH double cells under dark (b1) and UV (b2).

**Table 3.** The corrosion potential ( $V_{\text{corr}}$ ), current density ( $i_{\text{corr}}$ ) and open circuit potential (OCP) for: (i) Bare SS400 sample in NaCl and Na<sub>2</sub>S-NaOH double cells, (ii) SS400 Amorphous in NaCl double cells, (iii) SS400 Amorphous in NaCl and Na<sub>2</sub>S-NaOH double cells.

Sample	Condition	$V_{\text{corr}}$ (V)	$i_{\text{corr}}$ (A·cm <sup>-2</sup> )	OCP (V)
(i) SS400	UV	-0.537	6.92E-05	-0.555
	Dark	-0.368	8.19E-08	-0.433
(ii) SS400 Amorphous in NaCl	UV	-0.473	3.15E-05	-0.503
	Dark	-0.487	1.53E-05	-0.494
(iii) SS400 Amorphous in Na <sub>2</sub> S	UV	-0.595	1.44E-04	-0.533
	Dark	-0.561	1.28E-04	-0.559

The voltages of the samples with the Na<sub>2</sub>S-NaOH solution in the photoelectrolytic cell are more negative than those with the NaCl in the photoelectrolytic cell. Similarly, the current densities of the samples with the Na<sub>2</sub>S-NaOH solution in the photoelectrolytic cell are also 10 times higher. These were similarly observed in Ref. [50], which explained that Na<sub>2</sub>S could be used to prevent the recombination of EHP's by reacting of produced holes with S<sup>2-</sup> and the excitation of generated electrons into the CB, resulting in a more negative potential and higher current density.

The photoelectrochemical effect on the microstructures and surfaces of the samples in the double-cell system were investigated, as shown in Figure 12 and Figure 13. For the double-cell system with the NaCl solutions in both corrosion and photoelectrolytic cells, the bare sides in the NaCl corrosion cell were corroded with pitting and uniform corrosion, under either dark (Figure 12(c) and Figure 13(c)) or UV (Figure 12(d) and Figure 13(d)). For the ZnO-coated side in the NaCl photoelectrolytic cell, the ZnO-coated SS400 sides appeared to be stable without visible sign of corrosion under either dark (Figure 12(i) and Figure 13(i)) or UV (Figure 12(j) and Figure 13(j)).

For the double-cell system with the NaCl in the corrosion cell and the Na<sub>2</sub>S-NaOH solution in the photoelectrolytic cell, the ZnO-coated sides in the photoelectrolytic cells appeared to be stable under either dark (Figure 12(k) and Figure 13(k)) or UV (Figure 12(l) and Figure 13(l)). On the other hand, the different corrosion behaviors on the bare SS400 side in the corrosion cell, as evident in Figure 12(e-f)

and Figure 13(e-f). Under dark conditions, the bare SS400 side appeared to be corroded, as evident in Figure 12(e) and Figure 13(e). With the UV illumination, the bare SS400 side appeared to be stable without visible corrosion, as apparent in Figure 12(f) and Figure 13(f). The UV photocathodic protection seemed to be effective for the bare SS400 side in the corrosion cell with its opposite ZnO-coated side immersed in the photoelectrolytic cell of the Na<sub>2</sub>S-NaOH solution. As demonstrated in Ref. [41], the presence of Na<sub>2</sub>S in the photoelectrolytic cell helped capture photogenerated holes and prevent electron-hole recombination, resulting in the photocathodic protection of ZnO films for a carbon steel.

The concept of the photocathodic protection mechanism of ZnO photocatalytic to provide photogenerated EHP on the hot rolled steel SS400 under light illumination for the double-cell systems is illustrated in Figure 14. According to Ref. [41], under UV illumination, EHP can be generated in the ZnO coating. It has been reported that Na<sub>2</sub>S is an effective hole scavenger. The redox potential of S/S<sup>2-</sup> in Na<sub>2</sub>S-NaOH solution is more negative than that of O<sup>2</sup>/H<sub>2</sub>O in NaCl solution. As a result, in the Na<sub>2</sub>S-NaOH, holes can oxidize S<sup>2-</sup> in the electrolyte to form S, as described in the following reaction:



The electron also react with H<sup>+</sup> to form H<sub>2</sub>:

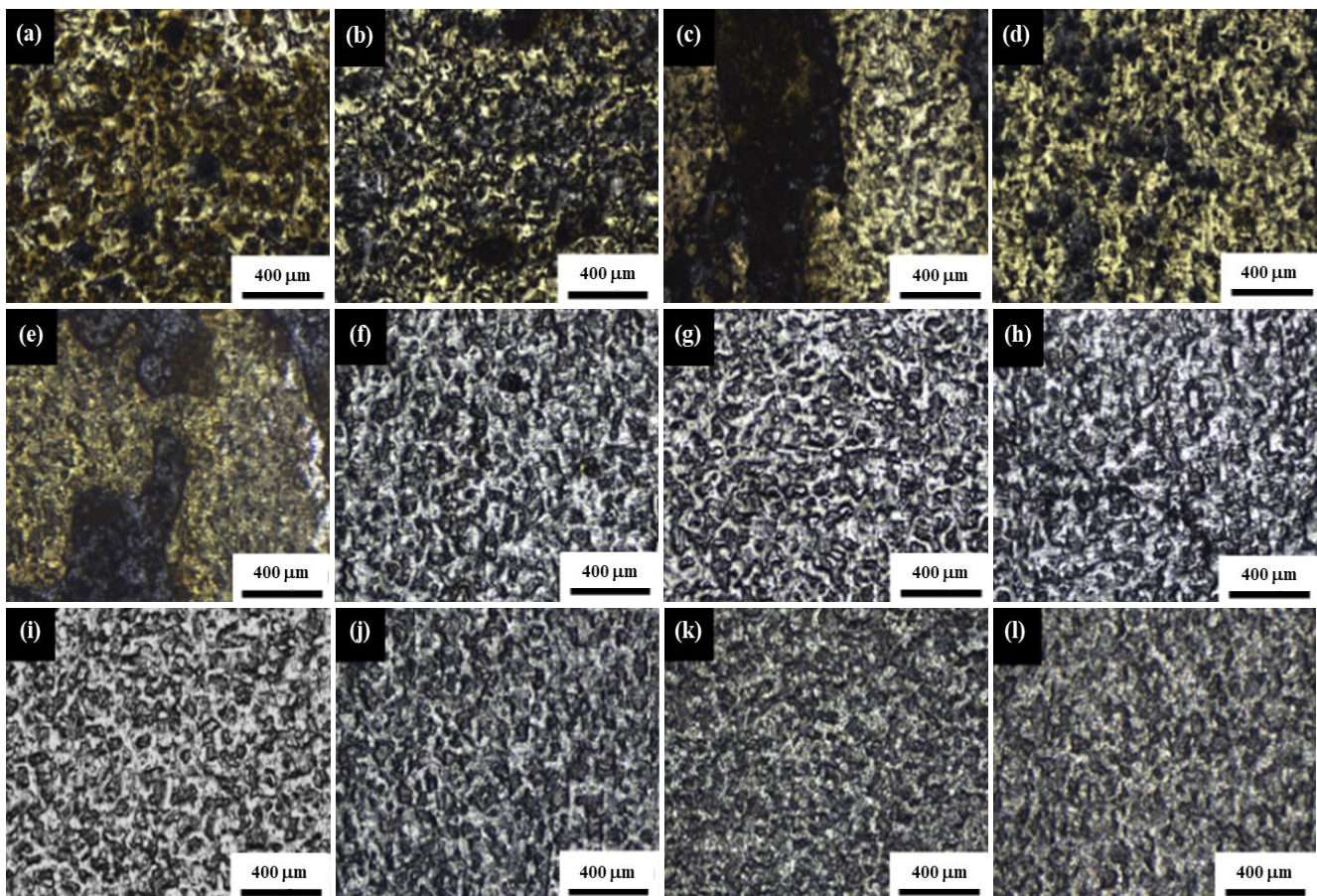


**Figure 12.** OM microstructures of the samples after the linear polarization measurement in the double-cell system. Bare SS400 in NaCl and Na<sub>2</sub>S-NaOH double cells: (a)-(b) and (g)-(h). SS400 Amorphous in NaCl double cells: (c)-(d) and (i)-(j). SS400 Amorphous in NaCl and Na<sub>2</sub>S-NaOH double cells: (e)-(f) and (k)-(l).

In the photoelectrolytic cell of the Na<sub>2</sub>S-NaOH solution, the band alignment of the SS400 substrate and the ZnO-coating film forms Schottky contact effect. Under UV illumination, the electrons are photo-generated in ZnO film, raising the Fermi level of the ZnO. As a result, the SS400 has a Fermi level lower than that of the ZnO film and the photogenerated electrons can be transferred from ZnO coating to the SS400 [60]. The transferred electrons could be used for the reaction with NaCl in the corrosion cell side to protect the SS400 bare side of SS400. The photogenerated holes in the ZnO film could react with S<sup>2-</sup> ion in the Na<sub>2</sub>S-NaOH solution to prevent

the recombination of electron-hole pairs. As a result, the SS400 bare side in the corrosion cell could be protected photocathodically under UV illumination in the electrolytic cell, as evident in Figure 12(f) and Figure 13(f).

Finally, the linear polarizations of the bare SS400 samples (with no ZnO coating on either side) under dark and UV conditions were measured. The linear polarization curves of SS400 samples with NaCl at corrosion cell and Na<sub>2</sub>S-NaOH at photoelectrolytic cell, under dark and UV conditions in a double cell system are shown in Figure 15(a) and (b), respectively. The corrosion potential (V<sub>corr</sub>) current density

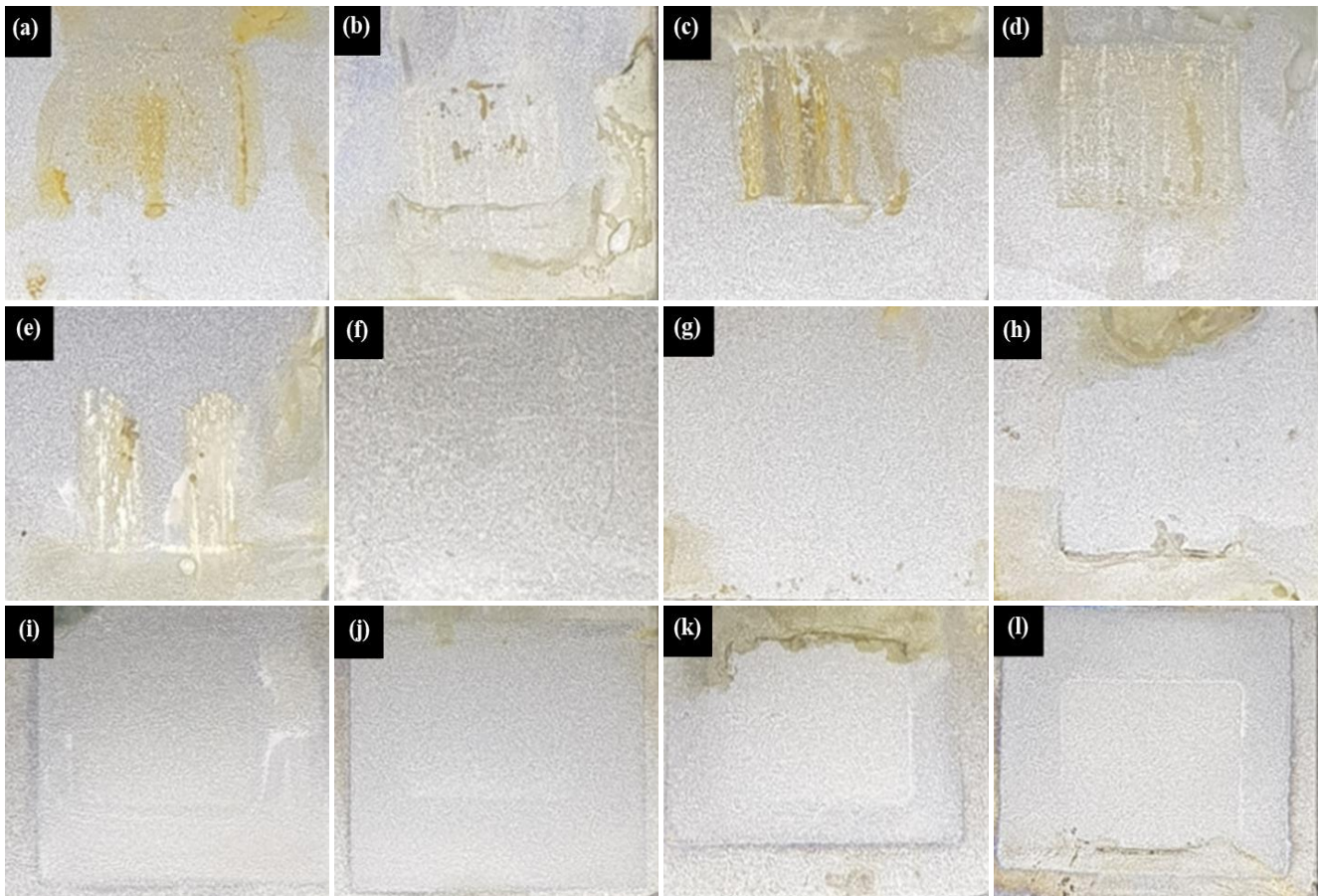


**Figure 13.** Digital pictures of the samples after the linear polarization measurement in the double-cell system. Bare SS400 in NaCl and Na<sub>2</sub>S-NaOH double cells: (a) – (b) and (g) – (h). SS400 Amorphous in NaCl double cells: (c) – (d) and (i) – (j). SS400 Amorphous in NaCl and Na<sub>2</sub>S-NaOH double cells: (e) – (f) and (k) – (l).

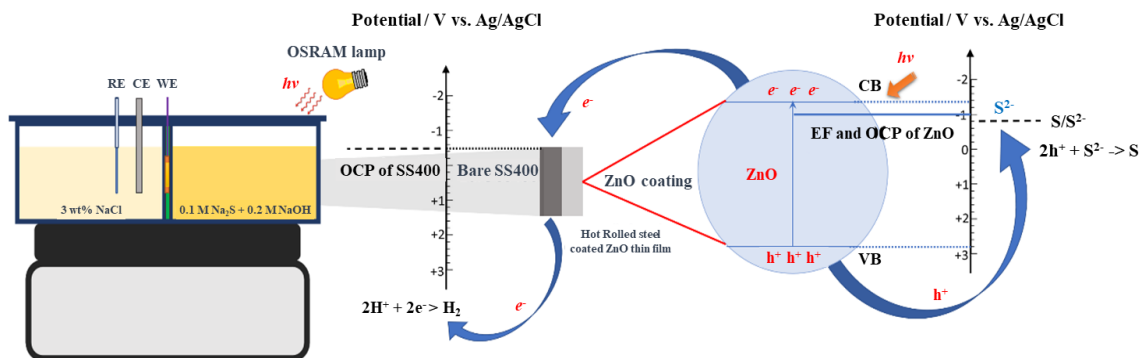


**Figure 14.** ZnO photocatalytic mechanism for the generation of the electron-hole pairs, which exhibit the photocathodic protection on the hot rolled steel SS400 under light illumination.

( $i_{\text{corr}}$ ) and open circuit potential (OCP) of SS400 sample with no ZnO coating on either side of the SS400 hot rolled steel, the corrosion cell of NaCl, and the photoelectrolytic cell of  $\text{Na}_2\text{S}$ -NaOH are summarized in Table 3(i) above. For the dark condition, the cathodic and anodic polarizations were observed with  $V_{\text{corr}}$  of -0.368 V (vs. Ag/AgCl), while, for the UV condition,  $V_{\text{corr}}$  was negatively shifted to -0.537 V (vs. Ag/AgCl). The current density also increased by 100 times with UV illumination. However, this negative shift of the potential and the rising current density under UV on did not provide photocathodic protection, as the samples' bare sides were thoroughly corroded, as evident in the microstructural and surface investigations, (Figure 12(a), (b) and Figure 13(a), (b)). In this case without any ZnO coating, the negative shift of  $V_{\text{corr}}$  and an increase of  $i_{\text{corr}}$  under UV illumination may have the negative side effect and the corrosion rate could be accelerated by the UV on the bare SS400, which worsen the corrosion behavior.

The photocathodic protection performance of ZnO appeared to be different between NaCl and  $\text{Na}_2\text{S}$ -NaOH photoelectrolytic cells, due to the difference of ZnO Fermi energy level and the redox potential under different ZnO/electrolyte interfaces. As described in Figure 14 above, after the ZnO was exposed to an electrolyte, the new Fermi energy level will be between the original ZnO Fermi energy level and the redox potential of the electrolyte. For NaCl electrolyte, the Fermi energy will be lower (more positive electrochemical potential), as the redox potential of  $\text{O}_2/\text{H}_2\text{O}$  in NaCl solution is more positive than the original ZnO Fermi energy potential. For the  $\text{Na}_2\text{S}$ -NaOH electrolyte, the ZnO Fermi energy will be higher (more negative electrochemical potential), because the redox potential of  $\text{S}/\text{S}^{2-}$  in  $\text{Na}_2\text{S}$ -NaOH is more negative than the ZnO Fermi energy potential. In order for photocathodic protection to be effective, the ZnO Fermi level should be higher (more negative) than that of the bare side steel. So, photo-generated electrons from ZnO can be transported from higher-FE ZnO side to the lower-FE bare steel side for cathodic protection [41]. However, for ZnO in NaCl photoelectrolytes, the FE level was shifted lower (more positive potential) and close to the FE level of the bare SS400 side. So, the photo-generated electrons in the CB of ZnO may not overcome the energy barrier between coated side and bare side, the electron transfers from ZnO to bare SS400 may be ineffective and, hence, the photocathodic protection performance for NaCl photoelectrolyte is lower than  $\text{Na}_2\text{S}$ -NaOH photoelectrolyte.

The different results between single-cell and double-cell system are due to different photocathodic mechanism processes. The single-cell system was designed to study a direct photocathodic reaction between one surface (either bare SS400 or ZnO coating) and a specific electrolyte (either NaCl or  $\text{Na}_2\text{S}$ -NaOH solutions). From the single-cell results, both SS400 and ZnO Amorphous were stable in  $\text{Na}_2\text{S}$ -NaOH solution under dark and UV condition with more negative  $V_{\text{corr}}$ , as opposed to SS400 and ZnO in the NaCl solution. The single-cell results demonstrate that ZnO film could exhibit better photocathodic behavior and stability in  $\text{Na}_2\text{S}$ -NaOH than in NaCl solution. For the double-cell system, it was designed to investigate the dual actions of the two sides (bare SS400 and Zn-coated sides) in different electrolytes. NaCl solution was used as a corrosion cell, because it is a normal corrosive atmosphere in real-world application. The  $\text{Na}_2\text{S}$ -NaOH was used in a photoelectrolytic cell to improve the photocathodic

protection performance of ZnO with  $\text{S}/\text{S}^{2-}$  hole scavenger and better ZnO stability, as demonstrated in the single-cell study. However, during the photoelectrochemical measurement for the double-cell system, two reactions on both corrosion and photoelectrolytic cells took place simultaneously, as shown in Figure 14. As a result, the photoelectrochemical results (voltage and current density) of the double-cell system were different from those of the single-cell system. Yet, for both single-cell and double-cell systems, the difference in photocathodic performances for varying electrolytes correspond well. For both single-cell and double-cell systems, ZnO coating in  $\text{Na}_2\text{S}$ -NaOH solution exhibited better photocathodic performance and more stable than ZnO coating in NaCl solution. For both single-cell and double-cell systems, under UV on,  $V_{\text{corr}}$  was shifted more negatively and  $i_{\text{corr}}$  was increased in  $\text{Na}_2\text{S}$ -NaOH than in NaCl solution.

The performance of ZnO photocathodic protection in this work were compared with prior work of ZnO coating on a different substrate. From Ref [48], The ZnO coating on an AISI type 304 stainless steel (SS304), in a 3% NaCl solution was investigated. The results demonstrated that under dark and UV condition, the  $i_{\text{corr}}$  was increased from  $6.0 \times 10^{-9} \text{ A}\cdot\text{cm}^{-2}$  (dark) to  $2.6 \times 10^{-5} \text{ A}\cdot\text{cm}^{-2}$  (UV) and  $V_{\text{corr}}$  was negatively shifted from -0.295 V vs. Ag/AgCl (dark) to -0.425 V vs. Ag/AgCl (UV). From Ref [58], the ZnO nanoparticle coating on SS304, in a 3.5 wt% NaCl solution, was investigated. The results showed that the  $i_{\text{corr}}$  was increased from  $9.7 \times 10^{-8} \text{ A}\cdot\text{cm}^{-2}$  (dark) to  $2.1 \times 10^{-7} \text{ A}\cdot\text{cm}^{-2}$  (UV) and the  $V_{\text{corr}}$  was negatively shifted from -0.200 V vs. Ag/AgCl (dark) to -0.252 V vs. Ag/AgCl (UV). From Ref [61], the ZnO nanoparticle coating on SS304 in a 3.5 wt% NaCl solution was investigated. The result showed that, with UV on, the  $i_{\text{corr}}$  and  $V_{\text{corr}}$  were  $1.34 \times 10^{-6} \text{ A}\cdot\text{cm}^{-2}$  and -0.246 V vs. Ag/AgCl, respectively. From the three prior work [48,58,61], with ZnO coating on SS304, the  $i_{\text{corr}}$  under dark condition (no photocathodic effect) was lower than that of SS400 Amorphous in  $\text{Na}_2\text{S}$  (this work). Moreover, the  $V_{\text{corr}}$  of bare SS400 sample under dark condition was more negative than that of SS304, because SS400 steel is less stable than SS304 stainless steel in NaCl solution. Under UV condition, the increasing  $i_{\text{corr}}$  and negatively-shifted  $V_{\text{corr}}$  of SS400 Amorphous in  $\text{Na}_2\text{S}$  was similar to the changes of  $i_{\text{corr}}$  and  $V_{\text{corr}}$  of ZnO-coating SS304.

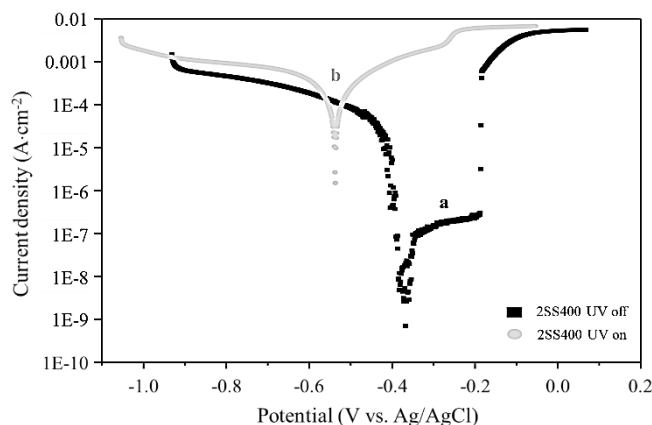


**Figure 15.** Linear polarization curves of the bare SS400 samples (no ZnO coating on either side) in the double-cell system, with the corrosion cell of the NaCl solution and the photoelectrolytic cell of the  $\text{Na}_2\text{S}$ -NaOH solution, under dark (a), and UV condition (b).

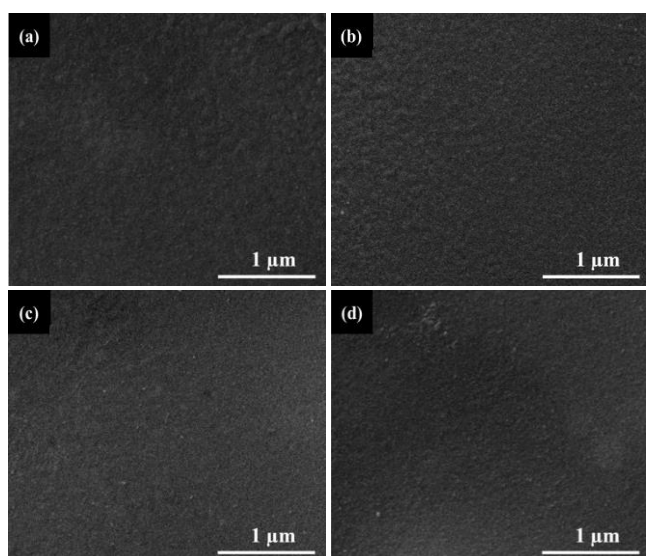


**Figure 16.** SEM microstructures of the amorphous ZnO coatings after the linear polarization measurement in the double-cell system. ZnO in Na<sub>2</sub>S-NaOH photoelectrolytic solution, under dark (a) and UV (b). ZnO in NaCl photoelectrolytic solution, under dark (c), and UV (d).

Figure 16 shows the SEM microstructures of the amorphous ZnO thin films after the polarization test under dark and UV conditions. The amorphous ZnO-coated side in the photoelectrolytic cell of Na<sub>2</sub>S-NaOH under dark and UV conditions are shown in Figure 16(a) and (b), respectively. The amorphous ZnO-coated SS400 side in the photoelectrolytic cell of NaCl, under dark and UV conditions are shown in Figure 16(c) and (d), respectively. The ZnO thin films in the photoelectrolytic cell of either Na<sub>2</sub>S-NaOH or NaCl solution appeared to be stable with negligible dissolution under both dark and UV conditions. These microstructures agree with the OM microstructures and surface analyses in Figure 12 and Figure 13 above. Under the single-cell system, the ZnO coating was in the corrosion cell. The ZnO coating appeared to be dissolved in the NaCl solution, while stable in the Na<sub>2</sub>S-NaOH solution. On the other hand, under the double-cell solution, the ZnO coating was in the photoelectrolytic cell and did not directly react in the electrochemical reaction, which occurred in the corrosion cell. As a result, the ZnO coating appeared to be stable in the photoelectrolytic cell of either Na<sub>2</sub>S-NaOH or NaCl solution. The current ZnO coating techniques by the spray-pyrolysis technique can be applied for industrial-scale coatings due to the scalability of the spray technique. For further development, the stability of ZnO coating should be improved to meet the demands of industrial applications. For example, the hydrophobic characteristic may be integrated to the ZnO coating to improve the stability and corrosion resistance of the coatings [62,63]. Moreover, the hybrid coatings of charge-storage layer and the photocathodic ZnO layer have also gained a lot of attentions in order to sustain the photocathodic protection during dark period [64].

#### 4. Conclusions

The amorphous ZnO thin film was successfully coated on hot rolled steel SS400 by a spray pyrolysis technique at 200 °C for 10 minutes. For the single-cell system, the amorphous ZnO coating

show exhibited photocathodic protection to SS400 in a Na<sub>2</sub>S-NaOH solution under UV condition with increasing of  $i_{\text{corr}}$  from  $9.86 \times 10^{-6}$  A/cm<sup>2</sup> (dark) to  $8.57 \times 10^{-5}$  A/cm<sup>2</sup> (UV) and the negative shift of  $V_{\text{corr}}$  from -0.454 V vs Ag/AgCl (dark) to -0.687 V vs Ag/AgCl (UV). Under dark condition for the single-cell system, the ZnO coating showed good stability in a Na<sub>2</sub>S-NaOH solution, with the  $V_{\text{corr}}$  of -0.454 V vs Ag/AgCl (dark) and -0.687 V vs Ag/AgCl (UV). However, the ZnO coating was unstable and dissolved in the NaCl solution for the single-cell system with  $V_{\text{corr}}$  of -0.342 V vs Ag/AgCl (dark) and -0.348 V vs Ag/AgCl (UV). For the double-cell system, the ZnO coatings were stable in the photoelectrolytic cell of either NaCl solution or Na<sub>2</sub>S-NaOH solution. However, from the microstructural and surface analyses, the bare SS400 in the corrosion cell appeared to be photocathodically protected with no visible corrosion observed on the working surface, only when the opposing ZnO-coated side was immersed in the Na<sub>2</sub>S-NaOH photoelectrolytic cell. From the cathodic polarization analyses, the voltage and current density of the ZnO-coated side in the Na<sub>2</sub>S-NaOH photoelectrolytic cell under UV condition were -0.595 V vs. Ag/AgCl and  $1.44 \times 10^{-4}$  A/cm<sup>2</sup>, respectively, while  $V_{\text{corr}}$  and  $i_{\text{corr}}$  of the NaCl photoelectrolytic solution under UV condition were -0.473 V vs. Ag/AgCl and  $3.15 \times 10^{-5}$  A/cm<sup>2</sup>, respectively. The cathodic polarization analyses show that the electrochemical photocathodic characteristics of ZnO coating in the Na<sub>2</sub>S-NaOH cell is better than those of ZnO coating in the NaCl cell, because the voltage was more negatively shifted and the current density was higher for the Na<sub>2</sub>S-NaOH photoelectrolytic cell. The presence of Na<sub>2</sub>S in the photoelectrolytic cell can provided better photocathodic protection than the NaCl counterpart.

#### Acknowledgements

This research was funded by Kasetsart University Research and Development Institution (KURDI). RT thanks International Collaborative Education Program for Materials Technology, Education, and Researcher (ICE-Matter), AUN/SEED-Net, JICA for the international conference support. PW thanks to Faculty of Engineering, Kasetsart University for his graduate scholarship grant.

#### References

- [1] B. Hou, X. Li, X. Ma, C. Du, D. Zhang, M. Zheng, W. Xu, D. Lu, and F. Ma, "The cost of corrosion in China," *npj Materials Degradation*, vol. 1, pp. 1-10, 2017.
- [2] Y. Bu, and J.-P. Ao, "A review on photoelectrochemical cathodic protection semiconductor thin films for metals," *Green Energy & Environment*, vol. 2, pp. 331-362, 2017.
- [3] B. A. Shaw, and R. G. Kelly, "What is corrosion?" *Electrochemical Society Interface*, vol. 15, pp. 24-26, 2006.
- [4] Z. C. Petrović, "Catastrophes caused by corrosion," *Military Technical Courier*, vol. 64, pp. 1048-1064, 2016.
- [5] X. Wei, C. Zhang, and X. Ling, "Effects of laser shock processing on corrosion resistance of AISI 304 stainless steel in acid chloride solution," *Journal of Alloys and Compounds*, vol. 723, pp. 237-242, 2017.

- [6] O. M. Alyousif, and R. Nishimura, "The stress corrosion cracking behavior of austenitic stainless steels in boiling magnesium chloride solutions," *Corrosion Science*, vol. 49, pp. 3040-3051, 2007.
- [7] O. M. Alyousif, and R. Nishimura, "On the stress corrosion cracking and hydrogen embrittlement of sensitized austenitic stainless steels in boiling saturated magnesium chloride solutions: Effect of applied stress," *Corrosion Science*, vol. 50, pp. 2919-2926, 2008.
- [8] D. Dwivedi, K. Lepková, and T. Becker, "Carbon steel corrosion: a review of key surface properties and characterization methods," *RSC Advances*, vol. 7, pp. 4580-4610, 2017.
- [9] J. Hu, Z. C. Guan, Y. Liang, J. Z. Zhou, Q. Liu, H. P. Wang, H. Zhang, and R. G. Du, "Bi<sub>2</sub>S<sub>3</sub> modified single crystalline rutile TiO<sub>2</sub> nanorod array films for photoelectrochemical cathodic protection," *Corrosion Science*, vol. 125, pp. 59-67, 2017.
- [10] Z. C. Guan, X. Wang, P. Jin, Y. Y. Tang, H. P. Wang, G. L. Song, and R. G. Du, "Enhanced photoelectrochemical performances of ZnS-Bi<sub>2</sub>S<sub>3</sub>/TiO<sub>2</sub>/WO<sub>3</sub> composite film for photocathodic protection," *Corrosion Science*, vol. 143, pp. 31-38, 2018.
- [11] W. X. Sun, S. W. Cui, N. Wei, S. G. Chen, Y. P. Liu, and D. A. Wang, "Hierarchical WO<sub>3</sub>/TiO<sub>2</sub> nanotube nanocomposites for efficient photocathodic protection of 304 stainless steel under visible light," *Journal of Alloys and Compounds*, vol. 749, pp. 741-749, 2018.
- [12] H. Li, X. Wang, L. Zhang, and B. Hou, "Preparation and photocathodic protection performance of CdSe/reduced graphene oxide/TiO<sub>2</sub> composite," *Corrosion Science*, vol. 94, pp. 342-349, 2015.
- [13] C. X. Lei, Z. D. Feng, and H. Zhou, "Visible-light-driven photo-generated cathodic protection of stainless steel by liquid-phase-deposited TiO<sub>2</sub> films," *Electrochimica Acta*, vol. 68, pp. 134-140, 2012.
- [14] N. Barati, M. A. F. Sani, and H. Ghasemi, "Photocathodic protection of 316L stainless steel by coating of anatase nanoparticles," *Protection of Metals and Physical Chemistry of Surfaces*, vol. 49, pp. 109-112, 2013.
- [15] M. K. Sahnesarayi, H. Sarpoolaky, and S. Rastegari, "Effect of heat treatment temperature on the performance of nano-TiO<sub>2</sub> coating in protecting 316L stainless steel against corrosion under UV illumination and dark conditions," *Surface and Coatings Technology*, vol. 258, pp. 861-870, 2014.
- [16] H. Deng, M. C. Huang, W. H. Weng, and J. C. Lin, "Photocathodic protection of iron oxide nanotube arrays fabricated on carbon steel," *Surface and Coatings Technology*, vol. 266, pp. 183-187, 2015.
- [17] S. S. Ge, Q. X. Zhang, X. T. Wang, H. Li, L. Zhang, and Q. Y. Wei, "Photocathodic protection of 304 stainless steel by MnS/TiO<sub>2</sub> nanotube films under simulated solar light," *Surface and Coatings Technology*, vol. 283, pp. 172-176, 2015.
- [18] J. Hu, Y. F. Zhu, Q. Liu, Y. B. Gao, R. G. Du, C. J. Lin, and SnO<sub>2</sub>, "Nanoparticle films prepared by pulse current deposition for photocathodic protection of stainless steel," *Journal of The Electrochemical Society*, vol. 162, pp. 161-166, 2015.
- [19] S. Cui, X. Yin, Q. Yu, Y. Liu, D. Wang, and F. Zhou, "Polypyrrole nanowire/TiO<sub>2</sub> nanotube nanocomposites as photoanodes for photocathodic protection of Ti substrate and 304 stainless steel under visible light," *Corrosion Science*, vol. 98, pp. 471-477, 2015.
- [20] J. Zhang, J. Hu, Y. F. Zhu, Q. Liu, H. Zhang, R. G. Du, and C. J. Lin, "Fabrication of CdTe/ZnS core/shell quantum dots sensitized TiO<sub>2</sub> nanotube films for photocathodic protection of stainless steel," *Corrosion Science*, vol. 99, pp. 118-124, 2015.
- [21] S. O. Moussa, and M. G. Hocking, "The photo-inhibition of localized corrosion of 304 stainless steel in sodium chloride environment," *Corrosion Science*, vol. 43, pp. 2037-2047, 2001.
- [22] Y. Ohko, S. Saitoh, T. Tatsuma, and A. Fujishima, "Photoelectrochemical anticorrosion and self-cleaning effects of a TiO<sub>2</sub> coating for type 304 stainless steel," *Journal of The Electrochemical Society*, vol. 148, pp. B24-B28, 2001.
- [23] J. M. Bastidas, and J. D. Scantlebury, "The influence of light on corrosion phenomena: the behaviour of mild steel in citric acid solution," *Corrosion Science*, vol. 26, pp. 341-347, 1986.
- [24] Y. Ohko, S. Saitoh, T. Tatsuma, and A. Fujishima, "Photoelectrochemical Anticorrosion Effect of SrTiO<sub>3</sub> for Carbon Steel," *Electrochemical and Solid-State Letters*, vol. 5, pp. B9-B12, 2002.
- [25] J. Yuan, and S. Tsujikawa, "Characterization of sol-gel-derived TiO<sub>2</sub> coatings and their photoeffects on copper substrates," *Journal of The Electrochemical Society*, vol. 142, pp. 3444-3450, 1995.
- [26] I. E. Paulauskas, J. E. Katz, G. E. Jellison Jr., N. S. Lewis, and L. A. Boatner, "Photoelectrochemical studies of semiconducting photoanodes for hydrogen production via water dissociation," *Thin Solid Films*, vol. 516, pp. 8175-8178, 2008.
- [27] J. Mayne, "Paints for the protection of steel—A Review of research into their action," *British Corrosion Journal*, vol. 5, pp. 160, 1970.
- [28] S. Li, and J. Fu, "Improvement in corrosion protection properties of TiO<sub>2</sub> coatings by chromium doping," *Corrosion Science*, vol. 68, pp. 101-110, 2013.
- [29] M. J. Zhou, N. Zhang, L. Zhang, and J. H. Yan, "Photocathodic protection properties of TiO<sub>2</sub>-V<sub>2</sub>O<sub>5</sub> composite coatings," *Materials and Corrosion*, vol. 64, pp. 996-1000, 2013.
- [30] M. Li, S. Luo, P. Wu, and J. Shen, "Photocathodic protection effect of TiO<sub>2</sub> films for carbon steel in 3% NaCl solutions," *Electrochimica Acta*, vol. 50, pp. 3401-3406, 2005.
- [31] H. Li, X. Wang, Y. Liu, and B. Hou, "Ag and SnO<sub>2</sub> co-sensitized TiO<sub>2</sub> photoanodes for protection of 304SS under visible light," *Corrosion Science*, vol. 82, pp. 145-153, 2014.
- [32] H. Xu, W. Liu, L. Cao, G. Su, and R. Duan, "Preparation of porous TiO<sub>2</sub>/ZnO composite film and its photocathodic protection properties for 304 stainless steel," *Applied Surface Science*, vol. 301, pp. 508-514, 2014.
- [33] T. Imokawa, R. Fujisawa, A. Suda, and S. Tsujikawa, "Protection of 304 Stainless steel with TiO<sub>2</sub> coating," *Zairyo-to-Kankyo*, vol. 43, pp. 482-486, 1994.
- [34] R. Subasri, S. Deshpande, S. Seal, and T. Shinohara, "Evaluation of the Performance of TiO<sub>2</sub>-CeO<sub>2</sub> Bilayer Coatings as Photoanodes

- for Corrosion Protection of Copper,” *Electrochemical and Solid-State Letters*, vol. 9, pp. B1-B4, 2006.
- [35] Y. F. Zhu, L. Xu, J. Hu, J. Zhang, R. G. Du, and C. J. Lin, “Fabrication of heterostructured SrTiO<sub>3</sub>/TiO<sub>2</sub> nanotube array films and their use in photocathodic protection of stainless steel,” *Electrochimica Acta*, vol. 121, pp. 361-368, 2014.
- [36] J. Hu, Q. Liu, H. Zhang, C. D. Chen, Y. Liang, R. G. Du, and C. J. Lin, “Facile ultrasonic deposition of SnO<sub>2</sub> nanoparticles on TiO<sub>2</sub> nanotube films for enhanced photoelectrochemical performances,” *Journal of Materials Chemistry A*, vol. 3, pp. 22605-22613, 2015.
- [37] J. Lei, Q. Shao, X. Wang, Q. Wei, L. Yang, H. Li, Y. Huang, and B. Hou, “ZnFe<sub>2</sub>O<sub>4</sub>/TiO<sub>2</sub> nanocomposite films for photocathodic protection of 304 stainless steel under visible light,” *Materials Research Bulletin*, vol. 95, pp. 253-260, 2017.
- [38] J. Cui, and Y. S. Pei, “Enhanced photocathodic protection performance of Fe<sub>2</sub>O<sub>3</sub>/TiO<sub>2</sub> heterojunction for carbon steel under simulated solar light,” *Journal of Alloys and Compounds*, vol. 779, pp. 183-192, 2019.
- [39] H. Li, Y. H. Li, M. Wang, Z. Niu, X. T. Wang, and B. R. Hou, “Preparation and photocathodic protection property of ZnIn<sub>2</sub>S<sub>4</sub>/RGO/TiO<sub>2</sub> composites for Q235 carbon steel under visible light,” *Nanotechnology*, vol. 29, p. 435706, 2018.
- [40] H. Park, K. Y. Kim, and W. Choi, “Photoelectrochemical approach for metal corrosion prevention using a semiconductor photoanode,” *The Journal of Physical Chemistry B*, vol. 106, pp. 4775-4781, 2002.
- [41] M. Sun, Z. Chen, Y. Bu, J. Yu, and B. Hou, “Effect of ZnO on the corrosion of zinc, Q235 carbon steel and 304 stainless steel under white light illumination,” *Corrosion Science*, vol. 82, pp. 77-84, 2014.
- [42] S. Y. Arman, H. Omidvar, S. H. Tabaian, M. Sajjadnejad, S. Fouladvand, and S. Afshar, “Evaluation of nanostructured S-doped TiO<sub>2</sub> thin films and their photoelectrochemical application as photoanode for corrosion protection of 304 stainless steel,” *Surface and Coatings Technology*, vol. 251, pp. 162-169, 2014.
- [43] J. Li, C. J. Lin, J. T. Li, Z. and Q. Lin, “A photoelectron-chemical study of CdS modified TiO<sub>2</sub> nanotube arrays as photoanodes for cathodic protection of stainless steel,” *Thin Solid Films*, vol. 519, pp. 5494-5502, 2011.
- [44] L. Xu, Y. F. Zhu, J. Hu, J. Zhang, Y. Z. Shao, R. G. Du, and C. J. Lin, “TiO<sub>2</sub> nanotube films prepared by anodization in glycerol solutions for photocathodic protection of stainless steel,” *Journal of The Electrochemical Society*, vol. 161, pp. 231-235, 2014.
- [45] G. X. Shen, Y. C. Chen, and C. J. Lin, “Corrosion protection of 316 L stainless steel by a TiO<sub>2</sub> nanoparticle coating prepared by sol-gel method,” *Thin Solid Films*, vol. 489, pp. 130-136, 2005.
- [46] G. X. Shen, Y. C. Chen, L. Lin, and C. J. Lin, “Study on a hydrophobic nano-TiO<sub>2</sub> coating and its properties for corrosion protection of metals,” *Electrochim. Acta*, vol. 50, pp. 5083-5089, 2005.
- [47] R. Subasri, and T. Shimohara, “The applicability of SnO<sub>2</sub> coatings for corrosion protection of metals,” *Electrochemical Solid-State Letter*, vol. 7, pp. B17-B20, 2004.
- [48] R. Techapiesancharoenkij, W. Sripiannem, K. Tongpul, C. Peamjharean, T. N. Wichean, T. Meesak, and P. Eiamchai, “Investigation of the photocathodic protection of a transparent ZnO coating on an AISI type 304 stainless steel in a 3% NaCl solution,” *Surface and Coatings Technology*, vol. 320, pp. 97-102, 2017.
- [49] A. Paracchino, V. Laporte, K. Sivula, M. Grätzel, and E. Thimsen, “Highly active oxide photocathode for photoelectrochemical water reduction,” *Nature Materials*, vol. 10, pp. 456-461, 2011.
- [50] Y. Yang, and Y. F. Cheng, “Factors affecting the performance and applicability of Sr-TiO<sub>3</sub> photoelectrodes for photoinduced cathodic protection,” *Journal of The Electrochemical Society*, vol. 164, pp. C1067-C1075, 2017.
- [51] Y. Yang, and Y. F. Cheng, “One-step facile preparation of ZnO nanorods as high-performance photoanodes for photoelectronchemical cathodic protection,” *Electrochimica Acta*, vol. 276, pp. 311-318, 2018.
- [52] S. Bee, A. Hamid, S. J. Teh, and C. W. Lai, “Photocatalytic water oxidation on ZnO: A Review,” *Catalysts*, vol. 7, pp. 93-107, 2017.
- [53] Y. Liang, Z. C. Guan, H. P. Wang, and R. G. Du, “Enhanced photoelectrochemical anticorrosion performance of WO<sub>3</sub>/TiO<sub>2</sub> nanotube composite films formed by anodization and electrodeposition,” *Electrochemistry Communications*, vol. 77, pp. 120-123, 2017.
- [54] K. L. Nardi, N. Yang, C. F. Dickens, A. L. Strickler, and S. F. Bent, “Creating highly active atomic layer deposited NiO electrocatalysts for the oxygen evolution reaction,” *Advanced Energy Materials*, vol. 5, p. 1500412, 2015.
- [55] M. Sun, Z. Chen, and J. Yu, “Highly efficient visible light induced photoelectrochemical anticorrosion for 304SS by Ni-doped TiO<sub>2</sub>,” *Electrochimica Acta*, vol. 109, pp. 13-19, 2013.
- [56] J. D. Merchant, and M. Cocivera, “Preparation and doping of zinc oxide using spray pyrolysis,” *Chemistry of Materials*, vol. 7, pp. 1742-1749, 1995.
- [57] S. A. Studenikin, N. Golego, and M. Cocivera, “Optical and electrical properties of undoped ZnO films grown by spray pyrolysis of zinc nitrate solution,” *Journal of Applied Physics*, vol. 83, pp. 2104-2111, 1998.
- [58] Y. Liu, Z. Zhu, and Y. Cheng, “An in-depth study of photocathodic protection of SS304 steel by electrodeposited layers of ZnO nanoparticles,” *Surface and Coatings Technology*, vol. 399, p. 126158, 2020.
- [59] W. Sripiannem, and R. Techapiesancharoenkij, “Effect of Al and Ga codoping on the morphological, electronic, and optical properties of ZnO transparent conductive thin films prepared by spray pyrolysis technique,” *Turkish Journal of Physics*, vol. 42, pp. 688-698, 2018.
- [60] D. Xu, M. Yang, Y. Liu, R. Zhu, X. Lv, C. Zhang, and B. Liu, “Fabrication of an innovative designed TiO<sub>2</sub> nanosheets/CdSe/polyaniline/graphene quaternary composite and its application as in situ photocathodic protection coatings on 304SS,” *Journal of Alloys and Compounds*, vol. 822, p. 153685, 2020.
- [61] Y. Liu, Z. Zhu, Y. Cheng, B. Wei, and Y. L. Cheng, “Effect of electrodeposition temperature on the thin films of ZnO nanoparticles used for photocathodic protection of SS304,” *Journal of Electroanalytical Chemistry*, vol. 881, p. 114945, 2021.

- [62] L. Hao, Y. Sirong, and H. Xiangxiang, "Preparation of a biomimetic superhydrophobic ZnO coating on an X90 pipeline steel surface," *New Journal of Chemistry*, vol. 39, pp. 4860-4868, 2015.
- [63] D. Lv, F. H. Shao, X. Gao, K. Lu, H. Lu, and H. Ma, "Fabrication and corrosion resistance properties of superhydrophobic coatings on iron and steel substrates by creating micro-/nano-structure and modifying rough surfaces," *RSC Advances*, vol. 6, pp. 93419-93427, 2016.
- [64] Y. Yang, Y.F. Cheng, "Bi-Layered CeO<sub>2</sub>/SrTiO<sub>3</sub> nanocomposite photoelectrode for energy storage and photocathodic protection," *Electrochimica Acta*, vol 253, pp. 134-141, 2017.